A diagram technique for Hubbard operators: the magnetic phase diagram in the (t-J) model

1990 J. Phys.: Condens. Matter 2 8905

(http://iopscience.iop.org/0953-8984/2/45/005)

J. Phys.: Condens. Matter 2 (1990) 8905–8923. Printed in the UK

A diagram technique for Hubbard operators: the magnetic phase diagram in the (t–J) model

Yu A Izyumov and B M Letfulov
Institute of Metal Physics, Ural Division of the USSR Academy of Sciences, 620219 Sverdlovsk GSP-170, USSR

Received 17 April 1990

Abstract. We construct a diagram technique for the (t–J) model Hamiltonian expressed in terms of Hubbard operators. This technique combines features of the diagram technique for normal Fermi systems and those of the diagram technique for the Heisenberg model with spin operators. The general graphic structure is identified for one-particle Green functions composed of Hubbard operators. The diagram technique for the (t–J) model has logical consistency, is reasonably simple and can serve as a working tool in exploring various properties of this model. To an approximation that resides in summing ladder-type diagrams with antiparallel electron lines, we calculate the system's magnetic susceptibility. A formula of a novel type is derived which reflects the dual nature of the magnetic states in the Hubbard model; this duality manifests itself in the presence of a localised and an itinerant contribution in the bare susceptibility. We trace how the relative value of the localised contribution varies as the electron concentration is increased from 0 to 1. It is found that the localised contribution starts increasing dramatically in the vicinity of $n = \frac{2}{3}$. In consequence, with $n > \frac{2}{3}$, the paramagnetic phase of the system becomes unstable with respect to the occurrence of ferromagnetic or antiferromagnetic ordering. A magnetic phase diagram for zero temperature is constructed on the (t/U, n) plane.

1. Introduction

Despite a large amount of published work [1–6] devoted to the study of possible magnetic states in the three-dimensional Hubbard model, the problem is still far from being resolved and many results are at variance. The reason for the slow progress in this area lies in the extreme complexity of the model Hamiltonian, expressed in terms of Hubbard operators, and in the absence of a regular perturbation theory, for example a diagram technique, for the Hamiltonian involved. Strictly speaking, such a technique has long been available [7–11], and the most consistent exposition of it has been provided in a book [12]. However, the aforementioned technique is too complicated and therefore not very constructive.

Recently, the (t–J) model has come into extensive use, which corresponds to the limit $U \gg t$ of the initial Hubbard model, especially in the context of the non-phonon mechanisms of high-T_c superconductivity [13]. The Hamiltonian of the (t–J) model is somewhat simpler, for it contains no Hubbard operators describing electron pairs on a site. The purpose of the present paper is to construct a diagram technique for the Hamiltonian of the (t–J) model and to explore the system's dynamic magnetic susceptibility with the aid of the technique developed. The diagram technique rests, of

0953-8984/90/458905 + 19 $03.50

course, on Wick's theorem for Hubbard operators, which was formulated earlier [7–11]. The latter expresses the algorithm of calculating averages of a chronological product of Hubbard operators by a successive reduction to averages of the least number of operators. Such reduction is possible because the commutator (or anticommutator) of two Hubbard operators is itself one of the Hubbard operators. This is reminiscent of the situation with spin operators for which the commutator of two operators is a third spin operator.

The diagram technique for spin operators dates back to [14] and has been successfully applied to various problems of magnetism theory (see e.g. the book [12], where many of its applications are given). The same technique with Hubbard operators for the (t–J) model is a peculiar combination of the technique with spin operators and the standard technique for Fermi systems [15]. In section 2 of the present paper general principles of this technique are formulated and in section 3 we derive diagram series for one-particle Green functions constructed from Fermi-like and Bose-like Hubbard operators. For these, it has been possible to find (section 3) a very general graphic structure. It has turned out that the exact one-particle Green function is depicted by a sum of several graphic terms, one of which corresponds to the Dyson part in the sense that the Dyson equation can be written for this term, just as for ordinary Fermi or Bose systems. The other terms contain what we call terminal parts, which are attached to the Dyson line either from the left or from the right, as well as at both ends of the line. These terminal diagrams prove to be highly essential and can change the poles of the Green function.

The exposition of these sections of the paper may seem too cursory; however, they furnish the prerequisites for practical work in the technique with Hubbard operators. Some details of the technique are also described in [12].

The technique that we have constructed possesses great generality and high effectiveness and can be instrumental in studying various properties of the (t–J) model. The present paper (sections 4 and 5) investigates magnetic properties of the system. Specifically, we calculate the dynamic susceptibility of the system in the paramagnetic phase and explore the system's instability with respect to the occurrence of ferromagnetic and antiferromagnetic order. The question about the occurrence of ferromagnetism in the Hubbard model was posed by Hubbard himself, who has shown that in the simplest approximation (Hubbard-1) a ferromagnetic ordering is impossible whatever the electron concentration n (number of electrons per site), at least in cubic lattices. Improved approximations ([2–5] and other authors) have shown that in this model the ferromagnetism is liable to occur over a certain interval of concentrations n. However, there are substantial discrepancies between these results, for instance in the issue about the bounds of the interval within which the ferromagnetic state exists and about the type of ordering (saturated or non-saturated ferromagnetism). These discrepancies arise apparently from the various approximations that are due to uncontrollable decouplings of chains of equations of motion for the Green functions. In this context, particular importance attaches to individual exact results (e.g. Nagaoka's theorem [6]) or regular methods of perturbation theory (e.g. the diagram technique developed in the present paper).

As already stated, on the basis of the diagram technique developed, we have been able to ascertain the general structure of the spin Green functions, which enable the transverse and longitudinal susceptibilities to be obtained. All graphic structures for the Green functions are expressed in terms of four-leg and three-leg diagrams represented by graphic series. Perturbation theory has reduced virtually to an approximate calculation of the electron four-leg diagram.

For a concrete calculation of the four-leg diagram, we exploit an approximation that consists of summing electron loop diagrams. Such summation in the standard case of perturbation theory ($U \ll t$) corresponds to the random-phase approximation and leads to well known results [16] for the dynamic magnetic susceptibility. With the (t–J) model ($U \gg t$), the summation of all loop diagrams (four different loops arise in this case) also corresponds to the random-phase approximation but leads to a novel result for the magnetic susceptibility, in which features of a localised magnetism and those of an itinerant magnetism show up simultaneously. On the basis of the expression derived for the magnetic susceptibility, we have constructed on the (t/U, n) plane a phase diagram in which the regions of existence of the ferromagnetic and antiferromagnetic phases are delineated.

2. Perturbation theory with Hubbard operators

We consider the standard Hubbard model with the Hamiltonian

$$\hat{\mathcal{H}} = \sum_{ll'\sigma} t_{ll'} a_{l\sigma}^{+} a_{l'\sigma} + U \sum_{l} n_{l\uparrow} n_{l\downarrow} .$$

Under the conditions $U \gg t$ the Coulomb term is chosen as the Hamiltonian $\hat{\mathcal{H}}_0$, while the transfer Hamiltonian is viewed as $\hat{\mathcal{H}}_{\text{int}}$. As $\hat{\mathcal{H}}_0$ is diagonal with respect to the site indices, the Hamiltonian is conveniently expressed in terms of Hubbard operators. These operators, $X^{pq} = |p\rangle\langle q|$, are defined on the basis of four one-site functions, $|0\rangle$, $|+\rangle$, $|-\rangle$ and $|2\rangle$, which respectively describe states without an electron, with one electron and with two electrons on a given site. In terms of the operators X^{pq},

$$\hat{\mathcal{H}}_0 = \sum_{lp} \varepsilon_p X_l^{pp} \tag{2.1}$$

$$\hat{\mathcal{H}}_{\text{int}} = \sum_{ll'} t_{ll'} [(X_l^{+0} + X_l^{2-})(X_{l'}^{0+} + X_{l'}^{-2}) + (X_l^{-0} + X_l^{2+})(X_{l'}^{0-} + X_{l'}^{+2})]. \tag{2.2}$$

Here ε_p is the eigenvalue of the one-site contribution by $\hat{\mathcal{H}}_{0l}$ to $\hat{\mathcal{H}}_0$, the contribution being a diagonal matrix:

$$\hat{\mathcal{H}}_{0l} = \text{diag}\{0, -\mu - \tfrac{1}{2}h, -\mu + \tfrac{1}{2}h, U - 2\mu\} \tag{2.3}$$

(we have included in $\hat{\mathcal{H}}_0$ a term with an external magnetic field H, $h = g\mu_B H$ and a chemical potential μ).

We start by considering the limit $U \to \infty$, in which the state $|2\rangle$ does not occur, so that the total Hamiltonian (2.1), (2.2) reduces to

$$\hat{\mathcal{H}}_0 = \varepsilon_+ \sum_l X_l^{++} + \varepsilon_- \sum_l X_l^{--} \tag{2.4}$$

$$\hat{\mathcal{H}}_{\text{int}} = \sum_{ll'} t_{ll'} (X_l^{+0} X_{l'}^{0+} + X_l^{-0} X_{l'}^{0-}) \tag{2.5}$$

where $\varepsilon_\pm = -\mu \mp \frac{1}{2}h$. Thus, only nine of the sixteen operators X^{pq} remain for $U \to \infty$:

$$X^{+0}, X^{0+}, X^{-0}, X^{0-}; X^{+-}, X^{-+}; X^{00}, X^{--}, X^{++}. \tag{2.6}$$

The first four operators are Fermi-like (f-type), whereas X^{+-} and X^{-+} are Bose-like (b-type). The Hubbard operators satisfy the following permutation relations:

$$[X_l^{pq}, X_{l'}^{rs}]_\pm = (\delta_{qr} X_l^{ps} \pm \delta_{ps} X_{l'}^{rq}) \delta_{ll'}. \tag{2.7}$$

The upper symbol (anticommutator) is taken when both operators are of the f-type, while the lower symbol is taken when at least one of the operators is of the b-type, or diagonal. Instead of the initial diagonal operators, it is convenient to use linear combinations of these:

$$F_l^{\sigma 0} = X_l^{00} + X_l^{\sigma\sigma} \qquad B_l^{+-} = X_l^{++} - X_l^{--}. \tag{2.8}$$

The statistical mechanics of the model can be described with the aid of the Green functions due to Matsubara, which are statistical averages of the product of the Hubbard operators X_l^{pq} in the Heisenberg representation of $\tilde{X}_l^{pq}(\tau)$. Using the interaction representation, we write

$$\langle T(\tilde{X}_{l_1}^{p_1q_1}(\tau_1)\ldots\tilde{X}_{l_n}^{p_nq_n}(\tau_n))\rangle = \langle T(X_{l_1}^{p_1q_1}(\tau_1)\ldots X_{l_n}^{p_nq_n}(\tau_n)\sigma(\beta))\rangle_0/\langle\sigma(\beta)\rangle_0 \tag{2.9}$$

where all the notations are standard ones: $0 < \tau < \beta = 1/T$,

$$\tilde{X}_l^{pq}(\tau) = \mathrm{e}^{\tau\hat{\mathcal{H}}} X_l^{pq}\, \mathrm{e}^{-\tau\hat{\mathcal{H}}} \qquad X_l^{pq}(\tau) = \mathrm{e}^{\tau\hat{\mathcal{H}}_0} X_l^{pq}\, \mathrm{e}^{-\tau\hat{\mathcal{H}}_0} \tag{2.10}$$

$$\sigma(\beta) = T\exp\left(-\int_0^\beta \mathrm{d}\tau\, \hat{\mathcal{H}}_{\mathrm{int}}(\tau)\right). \tag{2.11}$$

From the form of equation (2.4) for $\hat{\mathcal{H}}_0$, we find an expression for the Hubbard operators in the interaction representation:

$$X_l^{pq}(\tau) = \mathrm{e}^{(\varepsilon_p - \varepsilon_q)\tau} X_l^{pq}. \tag{2.12}$$

In order to calculate averages of products of operators $X_l^{pq}(\tau)$, Wick's theorem has been proved, which permits averages of n operators to be reduced to a sum of averages of $n-1$ operators. A detailed exposition of the problem is available in the aforementioned book [12]. Here we quote only the final algorithm, which consists of the following: The average of the T-product of operators $X_l^{pq}(\tau)$ is broken up into a sum of terms with all possible pairings (couplings) of two operators. By a coupling we understand the equations

$$\overrightarrow{X_l^{pq}(\tau)X_{l'}^{p'q'}}(\tau') = \mp G^{pq}(\tau-\tau')[X_{l'}^{p'q'}, X_l^{pq}]_\pm(\tau') \tag{2.13}$$

$$\overrightarrow{X_l^{pq}(\tau)X_{l'}^{p'q'}}(\tau') = \mathcal{D}^{pq}(\tau-\tau')[X_{l'}^{p'q'}, X_l^{pq}]_-(\tau') \tag{2.14}$$

which are valid under the average sign $\langle\ldots\rangle_0$. The first equation is taken when X_l^{pq} is an f-operator, and the second when X_l^{pq} is a b-operator. In equation (2.13) the upper symbol is taken when the operator $X_{l'}^{p'q'}$ is of the f-type and the lower when the operator $X_{l'}^{p'q'}$ is of the b-type.

In these expressions, G and $\mathcal{D}$ are the Fermi and Bose Green functions, which are defined by the equations

$$G^{pq}(\tau) = -\mathrm{e}^{(\varepsilon_p-\varepsilon_q)\tau}\begin{cases} 1-f(\varepsilon_p-\varepsilon_q) & \tau>0 \\ -f(\varepsilon_p-\varepsilon_q) & \tau<0 \end{cases} \tag{2.15}$$

$$\mathcal{D}^{pq}(\tau) = -\mathrm{e}^{(\varepsilon_p-\varepsilon_q)\tau}\begin{cases} 1+N(\varepsilon_p-\varepsilon_q) & \tau>0 \\ N(\varepsilon_p-\varepsilon_q) & \tau<0 \end{cases} \tag{2.16}$$

with $f(x)$ and $N(x)$ being the Fermi and Bose distribution functions, respectively.

By virtue of the fact that the right-hand side of equations (2.13) and (2.14) involves

commutators or anticommutators of Hubbard operators, a pairing of two operators decreases the number of operators under the average sign by unity. As a result of a multiple repetition of the pairing procedure, the initial average of the T-product falls apart into a sum of terms in each of which only the diagonal operators (we denote these by Z_l^{pq}) enumerated in equation (2.8) will remain under the average sign. These averages can be calculated with the help of the generating functional

$$W = \mathrm{Sp}\left[\exp\left(-\beta\hat{\mathscr{H}}_0 + \sum_l \sum_{pq} \lambda_l^{pq} Z_l^{pq}\right)\right]$$
$$= \prod_l \left[\exp(\lambda_l^{+0} + \lambda_l^{-0}) + \exp(\lambda_l^{+0} - \beta\varepsilon_+) + \exp(\lambda_l^{-0} - \beta\varepsilon_-)\right] \tag{2.17}$$

using the formula (for operators Z_l^{pq} belonging to the same site)

$$\delta^{k-1}\langle Z^{p_1q_1}\rangle_0/\delta\lambda^{p_2q_2}\ldots\delta\lambda^{p_kq_k} = \langle(Z^{p_1q_1} - \langle Z^{p_1q_1}\rangle_0)\ldots(Z^{p_kq_k} - \langle Z^{p_kq_k}\rangle_0)\rangle_0 \tag{2.18}$$

where $\langle Z^{pq}\rangle_0$ stands for the averages of the operator Z_l^{pq}:

$$\langle Z^{pq}\rangle_0 = (1/W)\delta W/\delta\lambda^{pq}. \tag{2.19}$$

The averages calculated by equation (2.9) are broken up, in each order of perturbation theory, into a sum of terms, each of which is a product of the Green functions $G_\uparrow^0$, $G_\downarrow^0$, $\mathscr{D}^0$ (corresponding to G^{0+}, G^{0-}, $\mathscr{D}^{+-}$), as well as of the cumulants (2.18). We shall depict the Green functions by full lines and the quantity $t_{ll'}$ by a wavy line, according to the rule ($x = (l, \tau)$, $G_\sigma^0(x - x') = G_\sigma^0(\tau - \tau')\delta_{ll'}$, $\mathscr{D}^0(x - x') = \mathscr{D}^0(\tau - \tau')\delta_{ll'}$, $t(x - x') = t_{ll'}\delta(\tau - \tau')$):

$G_\uparrow^0(x - x') =$ 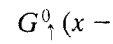 $G_\downarrow^0(x - x') =$

$\mathscr{D}^0(x - x') =$ 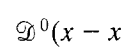 $t(x - x') =$ (2.20)

Cumulants of different order will be represented as small full circles (which we shall call 'circlets') enclosed in ovals. A circlet corresponds to a diagonal operator Z_l^{pq} that pertains to a site l, whereas an oval denotes that the site indices of all the operators Z_l^{pq} that are comprised in it coincide. Thus

$\langle Z_l^{pq}\rangle_0 =$  $\langle(Z_l^{pq} - \langle Z^{pq'}\rangle_0)(Z_{l'}^{p'q'} - \langle Z^{p'q'}\rangle_0)\rangle_0 =$ 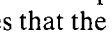 .... (2.21)

The resulting diagram technique has features of both the standard technique for Fermi or Bose operators and the spin operator technique (see [12]). The technique constructed employs a theorem of connectedness which enables us to transcribe the right-hand side of equation (2.9) as

$$\langle T(X_{l_1}^{p_1q_1}(\tau_1)\ldots X_{l_n}^{p_nq_n}(\tau_n)\sigma(\beta))\rangle_0^{\mathrm{conn}} \tag{2.22}$$

and thus to take into account only connected diagrams.

One important feature of the diagram technique for Hubbard operators must be noted. The Green lines (2.20) correspond to couplings of a pair of operators that go from an annihilation operator to a creation operator, as is normally adopted in diagram techniques. Significantly, the Hubbard operators (2.6) include several annihilation operators, for example X^{0+}, X^{0-}, X^{+-}, and pairing may begin with any one of these. Thus, with the graphic portrayal of the terms involved in equation (2.22) and found by

Wick's theorem, the resulting expressions have an ambiguous notation, which depends on the particular operator from which we have started [10]. To make the notation and the resulting diagram technique unequivocal, we need to choose for the non-diagonal operators X^{0+}, X^{0-}, X^{+-} a system of priorities that fixes the sequence of operations, i.e. indicates the operator with which to start pairing. The system of priorities is arbitrary and the choice of it is determined by the character of the physical problem.

We conclude this general section by ascertaining the meaning of the Green functions G^{pq} and $\mathcal{D}^{pq}$ introduced by equations (2.13) and (2.14). Using these equations, we calculate the expressions

$$\mathcal{G}^0_\sigma(x-x') = -\langle T(X^{0\sigma}_l(\tau)X^{\sigma 0}_{l'}(\tau'))\rangle_0 = G^0_\sigma(x-x')\langle F^{\sigma 0}\rangle_0 \tag{2.23}$$

$$\mathcal{D}^0_\perp(x-x') = -\langle T(X^{+-}_l(\tau)X^{-+}_{l'}(\tau'))\rangle_0 = \mathcal{D}^0(x-x')\langle B^{+-}\rangle_0 \tag{2.24}$$

which show the relation of the functions G^0_σ and $\mathcal{D}^0$ to the one-particle fermion and boson Green functions of the zero approximation. According to the rules proposed above, these relations have the following graphic representation:

$\mathcal{G}^0_\uparrow$ = 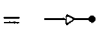 $\mathcal{G}^0_\downarrow$ = 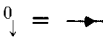 $\mathcal{D}^0_\perp$ = 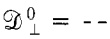 (2.25)

where the circlet at the end of the line respectively denotes a zeroth-order cumulant: $\langle F^{+0}\rangle_0$, $\langle F^{-0}\rangle_0$ and $\langle B^{+-}\rangle_0$. By the definitions (2.15) and (2.16), the corresponding expressions for the quantities G^0_σ and $\mathcal{D}^0$ in the momentum representation read

$$G^0_\sigma(\mathrm{i}\omega_n) = 1/(\mathrm{i}\omega_n - \varepsilon_\sigma) \qquad \omega_n = (2n+1)\pi T \tag{2.26}$$

$$\mathcal{D}^0(\mathrm{i}\omega_n) = 1/(\mathrm{i}\omega_n - h) \qquad \omega_n = 2n\pi T. \tag{2.27}$$

The cumulants that correspond to the Green functions (2.23) and (2.24) are

$$\langle F^{+0}\rangle = 1 - n_\downarrow \qquad \langle F^{-0}\rangle = 1 - n_\uparrow \qquad \langle B^{+-}\rangle = n_\uparrow - n_\downarrow \tag{2.28}$$

with n_σ being the mean number of electrons with spin σ on a single site.

3. Diagrammatic representation of one-particle Green functions in the limit

As in any diagram technique, the possible types of vertices and the rules of connecting these are determined by the structure of the Hamiltonian $\hat{\mathcal{H}}_{\mathrm{int}}$ (2.5) and do not depend on the Green function being calculated. In the technique with Hubbard operators the types of vertices depend, however, on the system of priorities or seniorities that has been adopted. In the present paper we adopt a seniority system defined by the symbolic formula

$$X^{0+} > X^{0-} > X^{+-} \tag{3.1}$$

where the operator on the left is senior to any one of the operators on the right and, in calculating the average of the T-product, it is necessary to start the pairing from the most senior operator. Possible vertex types in this system are shown in figure 1. Each vertex corresponds to one of the operators, X^{0+}, X^{+0}, X^{0-} and X^{-0}, involved in the expression (2.5) for $\hat{\mathcal{H}}_{\mathrm{int}}$. The occurrence of complicated vertices is typical of systems described by operators for which the commutator (or anticommutator) is not a c-number. For example, complicated vertices with two or three Green lines occur in the diagram technique for spin operators [12]. One feature peculiar to some vertices must be noted: When only Green lines enter the vertex (and none of the lines go out), the vertex

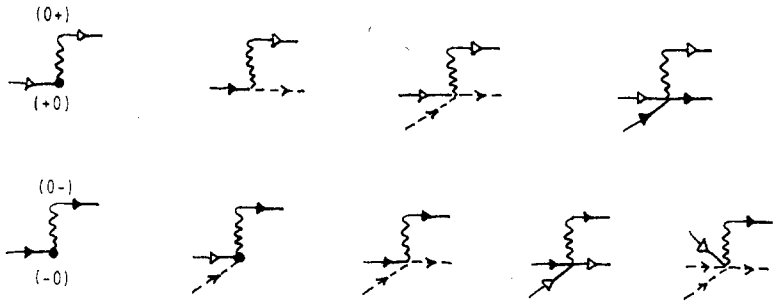

Figure 1. Possible inner vertices for Hamiltonian (2.5) in $X^{0+} > X^{0-} > X^{--}$ seniority system.

necessarily contains a circlet, which belongs to the end of one of the Green lines, the one that has been constructed on the junior operator of the seniority system adopted.

The graphic structures presented in figure 1 constitute the rules of the diagram technique. The form of the graphs for the Green funtions is determined by these rules and the operators $X_l^{pq}(\tau)$ assigning a given Green function (they determine the external vertices of diagrams). We have not defined a general rule for ascertaining the sign of a diagram. The sign of a diagram is convenient to find by appropriately unfolding the average according to Wick's theorem.

Let us consider a one-particle Green function that describes the propagation of an electron with a given spin projection:

$$\mathcal{G}_\sigma(x;x') = -\langle T(\tilde{X}_l^{0\sigma}(\tau)\tilde{X}_{l'}^{\sigma 0}(\tau'))\rangle. \tag{3.2}$$

To a zero approximation, these quantities are depicted by the first two graphs from (2.25). We give a graphic depiction of $\mathcal{G}_\uparrow$ in the first order of perturbation theory. This is

$\mathcal{G}_\uparrow =$ 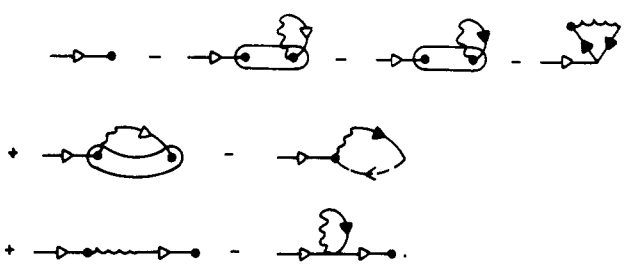 (3.3)

In the first row we have written out graphs that may be viewed as a thickening of the circlet •; that is, this row contains quantities $\langle F^{+0}\rangle_0$. The second row contains what are called terminal diagrams (also appearing in the technique for spin operators), in which the external (right-hand) vertex is separated from the end of the Green line

 .

The third row contains self-energy graphs. As can be readily seen, the topological fragments that arise in the subsequent orders are the same; therefore, an exact graphic depiction of the series (3.3) can be given. We label a full (thick) circlet

a full terminal part

and a full self-energy part

Then the series for the exact Green function can be represented by the equation

 (3.4)

where the thick fermion line satisfies the Dyson equation

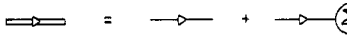 (3.5)

A similar graphic series occurs also for the function $\mathcal{G}_\downarrow$; this differs from the series (3.3) in the colour of the Green lines. With Δ_σ to denote the terminal part of the Green function $\mathcal{G}_\sigma$ and with Σ_σ to denote the self-energy part, the analytic representation of the exact Green function can be written in the form

$$\mathcal{G}_\sigma = (\langle F^{\sigma 0}\rangle + \Delta_\sigma)/[(G_\sigma^0)^{-1} - \Sigma_\sigma]. \tag{3.6}$$

The denominator (3.6) corresponds to the structure of a usual electron Green function satisfying the Dyson equation; the numerator reflects the fact that the anticommutator of the operators $X^{0\sigma}$ and $X^{\sigma 0}$, which define the Green function $\mathcal{G}_\sigma$, is not a c-number. An analogous structure is inherent in the one-particle spin Green function of a Heisenberg magnet in the spin operator technique [17].

To the quantity G_σ^0 corresponds the one-site Green function (2.15), which describes the localised perturbation of the electron state on a single site. The transition of an electron from one site to another is described by an infinite series of diagrams containing wavy lines. In the simplest case we have the series

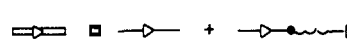 (3.7)

(a similar series holds also for the other spin orientation), to which corresponds the propagator

$$G_\sigma(\boldsymbol{k}_i\, \mathrm{i}\omega_n) = 1/[\mathrm{i}\omega_n - \xi_\sigma(\boldsymbol{k})] \tag{3.8}$$

where

$$\xi_\sigma(\boldsymbol{k}) = (1 - n_{-\sigma})\varepsilon(\boldsymbol{k}) + \varepsilon_\sigma \tag{3.9}$$

with $\varepsilon(\boldsymbol{k})$ being the band energy of an electron in the absence of a Coulomb interaction. In the nearest-neighbour approximation

$$\varepsilon(\boldsymbol{k}) = t\sum_{\Delta} \mathrm{e}^{\mathrm{i}k\Delta}. \tag{3.10}$$

The series (3.7) corresponds to the Hubbard-I approximation [1].

We now consider the Green function composed of Bose-like operators. This function has the form

$$\mathcal{D}_\perp(x - x') = -\langle T(\tilde{X}_l^{+-}(\tau)\tilde{X}_{l'}^{-+}(\tau'))\rangle \tag{3.11}$$

and describes the correlation of the transverse spin components, as the operators X^{+-} and X^{-+} are equivalent to the operators S^+ and S^-. In the zero approximation it is

depicted by the last graph of equation (2.25). Within the first order of perturbation theory we have

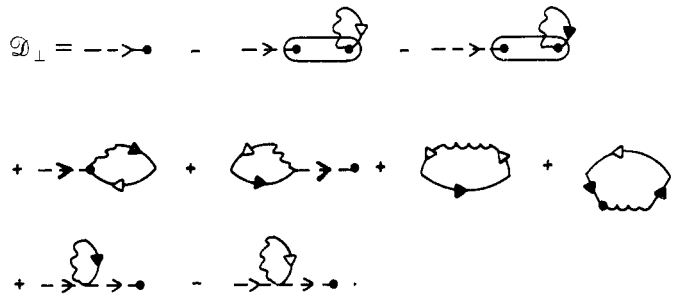

(3.12)

We see that two types of external vertices arise for the operator X^{+-} and there are two types of vertices corresponding to the operator X^{-+}. One of the vertex types is the beginning or end of the spin Green function

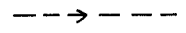

while the other corresponds to a vertex with an ingoing and an outgoing electron line, which have opposite spins. All the graphs of the series (3.12) can be sorted out according to the type of left-hand and right-hand external vertices. If we preliminarily perform the summation (3.7) in the electron lines and thus pass over to electron propagators, then we arrive at the following representation for $\mathscr{D}_\perp$:

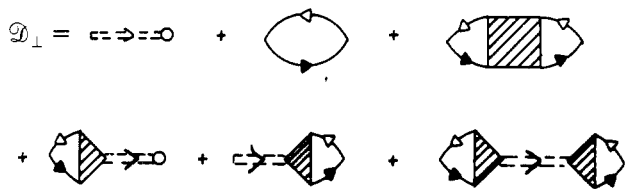

(3.13)

where the thickened spin Green function obeys the Dyson equation

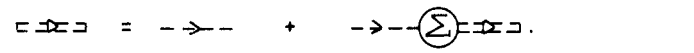

(3.14)

In expression (3.13) all the electron Green lines are exact propagators.

Thus, the function $\mathscr{D}_\perp$ is expressed in terms of vertex parts of three types, namely an electron four-leg diagram and two three-leg diagrams of a mixed type. The four-leg diagram and the three-leg diagrams are uncuttable along one spin line

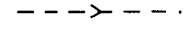

Solving equation (3.14), we write the expression for the transverse spin Green function in symbolic form:

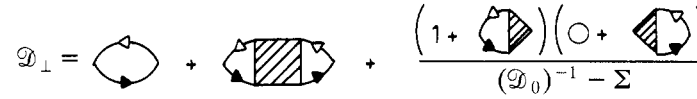

(3.15)

This notation reflects the mixed character of the dynamic susceptibility in the Hubbard model. The first two terms in equation (3.15) correspond to the contribution of the

itinerant electron states, whereas the last term describes rather the contribution of the localised states to the susceptibility as well as the superposition of both types of states.

We now introduce the Green function of the longitudinal spin components:

$$\mathcal{D}_{\parallel}(x;x') = \langle T(\tilde{B}_l^{+-}(\tau)\tilde{B}_{l'}^{+-}(\tau'))\rangle. \tag{3.16}$$

It falls apart into a sum of four functions of the form

$$\mathcal{K}^{\sigma\sigma'}(x;x') = \langle T(\tilde{F}_l^{\sigma 0}(\tau)\tilde{F}_{l'}^{\sigma' 0}(\tau'))\rangle. \tag{3.17}$$

We present a diagram series for one of these functions. For example,

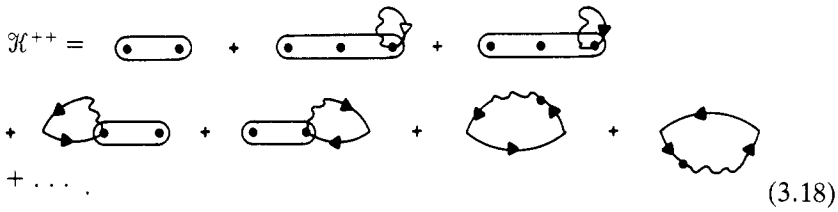

(3.18)

Analogous series can be written out also for other matrix elements. Passing to electron propagators, we represent these series as

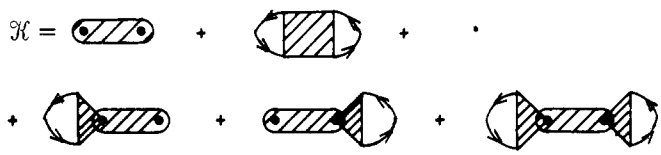

(3.19)

Each of the quantities involved here is a 2×2 matrix with respect to the spin indices σ and σ'. The quantities introduced here are

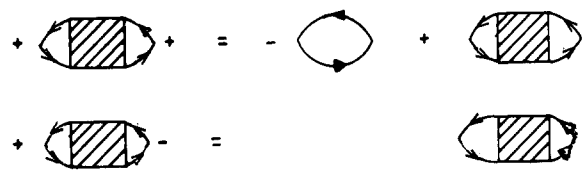

(3.20)

(the other two matrix elements are obtained from these quantities by changing the colour of the arrows). The symbol

denotes a thickened entity that has two external vertices of the type ●, i.e. vertices which correspond to the diagonal operator $F^{\sigma 0}$. For this entity we can set up an equation which has the structure of the Dyson equation:

(3.21)

where the irreducible part

is uncuttable along the quantity

 .

The quantity

has a matrix structure.

Thus, expressions (3.15), (3.19) and (3.21) tell us that the longitudinal and transverse Green functions in the hierarchy $X^{0+} > X^{0-} > X^{+-}$ have closely related structures and reflect the existence of three contributions: by the itinerant states, by the localised states and by the superposition of these states.

Up to this point we have considered the limit $U \to \infty$. At finite U, which, however, are sufficiently large, as before, for the small parameter $\kappa = t/U \ll 1$ to exist, excluding the electron pairs in the initial Hamiltonian (2.2) leads to the effective Hamiltonian [13]

$$\hat{\mathcal{H}}_{\text{eff}} = 4\kappa t \sum_{l\sigma\Delta} (\boldsymbol{S}_l \boldsymbol{S}_{l+\Delta} - \tfrac{1}{4}\hat{n}_l \hat{n}_{l+\Delta}) \tag{3.22}$$

where $\boldsymbol{S}_l$ is the spin operator and $\hat{n}_l = \hat{n}_{l\uparrow} + \hat{n}_{l\downarrow}$ the operator of the number of electrons in a site l. In terms of the Hubbard operators, the corresponding expression for this Hamiltonian is

$$\hat{\mathcal{H}}'_{\text{int}} = \sum_{ll'} J_{ll'} (X_l^{-+} X_{l'}^{+-} - X_l^{++} X_{l'}^{--}) \tag{3.23}$$

where

$$J_{ll'} = \kappa t \sum_{\Delta} \delta(l - l' - \Delta).$$

To obtain the total interaction Hamiltonian for the situation $U \gg t$, we need to add equation (3.23) to expression (2.5) for $\hat{\mathcal{H}}_{\text{int}}$. Inclusion of $\hat{\mathcal{H}}'_{\text{int}}$ leads to additional vertices, shown for the same system of priorities in figure 2. The dotted line in this figure refers to the quantity $J_{ll'}$. The Hamiltonian (3.23) says that the dotted line may join either vertices of the type $(-+)$ and $(+-)$ or vertices of the type $(++)$ and $(--)$.

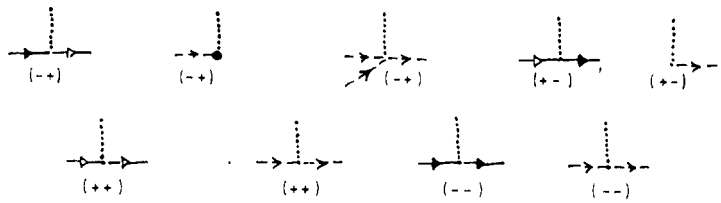

Figure 2. Possible inner vertices for Hamiltonian (3.23).

If we consider as the perturbation both terms, $\mathcal{H}_{\text{int}}$ and $\mathcal{H}'_{\text{int}}$, in the Hamiltonian (a situation corresponding to the (t–J) model), we shall see that there exist no vertices at which both interaction lines, dotted and wavy, converge. For this reason, the general graphic expressions for the Green functions (3.4), (3.13) and (3.19), obtained by taking account of only the kinetic term $\mathcal{H}_{\text{int}}$, hold good also in the general case where the Hamiltonian (3.23) is added to this term.

4. Dynamic paramagnetic susceptibility in the (t–J) model

In this section we consider the Green functions of the transverse and longitudinal spin components in the paramagnetic phase by invoking an approximation that corresponds

to the random-phase approximation (RPA). In this case the Green functions being studied are expressed via electron four-leg diagrams. As can be seen from figures 1 and 2, there are four bare purely electronic vertices:

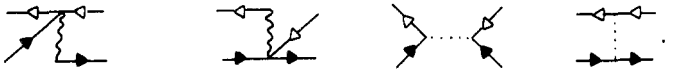

(4.1)

We choose an approximation in which ladder diagrams with antiparallel lines are summed. Normally, such summation corresponds to the RPA or the non-interacting mode approximation. For the four-leg diagram defining the function $\mathfrak{D}_\perp$ we set up the equation

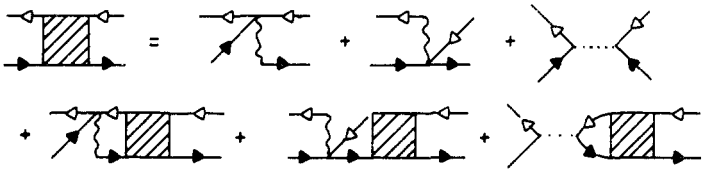

(4.2)

which allows for all the graphs with antiparallel lines; the graphs consist of individual loops joined together at one point, the same momentum k corresponding to each of the loops. There are four types of such loops, which pertain to the quantities $\Pi(k)$, $Q(k)$, $\Lambda(k)$ and $\Phi(k)$ (see the definitions below). Successive stringing of such loops corresponds to allowance for non-interacting modes. The last of the bare graphs (4.1) is dropped, because it only dresses the simple loops, connecting in them the electron lines with opposite spins and thereby perturbing the graphic structure of the RPA.

We introduce the analytic notation of the four-leg diagram:

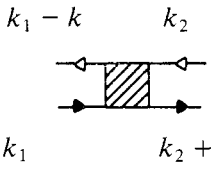

$$= \Gamma(k_1 - k, k_1; k_2 + k, k_2) \qquad k = (\boldsymbol{k}, \mathrm{i}\omega_n). \tag{4.3}$$

The integral equation (4.2) is easy to reduce to an algebraic one, and we can readily obtain the exact solution of it in the form

$$\Gamma(k_1 - k, k_1; k_2 + k, k_2) = [1/d_\perp(k)]\{\varepsilon(\boldsymbol{k}_1 - \boldsymbol{k})\varepsilon(\boldsymbol{k}_2 + \boldsymbol{k})\Pi(k) + \varepsilon(\boldsymbol{k}_1 - \boldsymbol{k})[1 - Q(k)] + \varepsilon(\boldsymbol{k}_2 + \boldsymbol{k})[1 - \Lambda(k)] + \Phi(k) + J(\boldsymbol{k})\} \tag{4.4}$$

with

$$d_\perp(k) = [1 - \Lambda(k)][1 - Q(k)] - \Pi(k)[\Phi(k) + J(\boldsymbol{k})] \tag{4.5}$$

$$\begin{pmatrix} \Pi(k) \\ Q(k) \\ \Lambda(k) \\ \Phi(k) \end{pmatrix} = \frac{1}{N}\sum_{k_1} \begin{pmatrix} 1 \\ \varepsilon(\boldsymbol{k}_1) \\ \varepsilon(\boldsymbol{k}_1 - \boldsymbol{k}) \\ \varepsilon(\boldsymbol{k}_1)\varepsilon(\boldsymbol{k}_1 - \boldsymbol{k}) \end{pmatrix} G^0_\uparrow(k_1 - k)G^0_\downarrow(k_1) \tag{4.6}$$

where we can take as $G_\sigma(k)$ expression (3.8).

We now define the three-point vertex parts

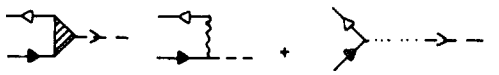

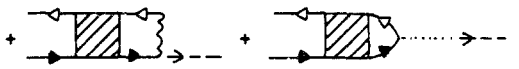

(4.7)

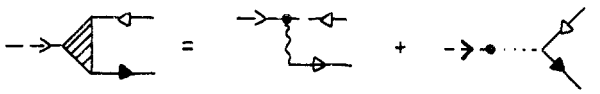

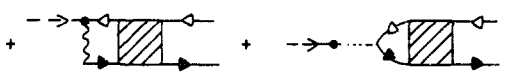

(4.8)

Let us call them γ_L and γ_R, respectively. Substituting into these expressions equation (4.4) for the four-leg diagram yields

$$\gamma_L(k_1 - k, k_1; k) = \{\varepsilon(\boldsymbol{k}_1 - \boldsymbol{k})[1 - Q(k)] + \Phi(k) + J(\boldsymbol{k})\}/d_\perp(k) \tag{4.9}$$

$$\gamma_R(k; k_2 + k, k_2) = \langle B^{+-}\rangle_0\{\varepsilon(\boldsymbol{k}_2 + \boldsymbol{k})[1 - \Lambda(k)] + \Phi(k) + J(\boldsymbol{k})\}/d_\perp(k). \tag{4.10}$$

We now can readily calculate the left-hand and right-hand terminal parts in expression (3.13) for the transverse Green function:

$$\equiv \mathcal{R}(k) = \langle B^{+-}\rangle_0\{Q(k)[1 - \Lambda(k)] + \Pi(k)[\Phi(k) + J(\boldsymbol{k})]\}/d_\perp(k) \tag{4.11}$$

$$\equiv \mathcal{L}(k) = \{\Lambda(k)[1 - Q(k)] + \Pi(k)[\Phi(k) + J(\boldsymbol{k})]\}/d_\perp(k) \tag{4.12}$$

and also the quantity

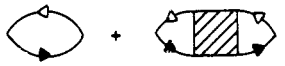

$$\equiv \pi(k) = \Pi(k)/d_\perp(k). \tag{4.13}$$

It remains for us to calculate the irreducible self-energy part in equation (3.14) for the spin Green function. This irreducible part is expressed through the three-point vertex part (4.8):

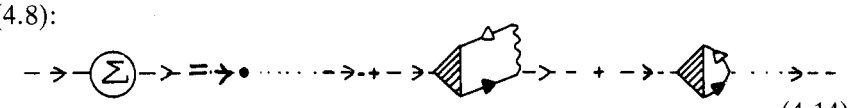

(4.14)

whence we obtain

$$\Sigma(k) = \langle B^{+-}\rangle_0[\Phi(k) + J(\boldsymbol{k})]/d_\perp(k). \tag{4.15}$$

Using expressions (3.13) and (3.14), we can easily obtain the final expression for the transverse Green function:

$$\mathcal{D}_\perp(k) = \frac{\langle B^{+-}\rangle_0\mathcal{D}^0(i\omega_n) + \Pi(k)}{[1 - \Lambda(k)][1 - Q(k)] - [\langle B^{+-}\rangle_0\mathcal{D}^0(i\omega_n) + \Pi(k)][\Phi(k) + J(\boldsymbol{k})]} \tag{4.16}$$

with $\mathcal{D}^0(i\omega_n)$ being the zero-approximation spin Green function defined by formula (2.27).

We proceed to consider the paramagnetic phase in the absence of an external magnetic field. Using two relations,

$$\langle B^{+-}\rangle_0 = \langle F^{+0}\rangle_0 - \langle F^{-0}\rangle_0 \qquad \langle F^{\sigma 0}\rangle_0 = n\frac{1+e^{-\beta\varepsilon_\sigma}}{1+e^{-\beta\varepsilon_+}+e^{-\beta\varepsilon_-}}$$

we calculate the limit

$$[\langle B^{+-}\rangle_0 \mathcal{D}^0(i\omega_n)]_{h\to 0} = -\tfrac{1}{2}\beta n n_0 \delta_{\omega_n,0} \tag{4.17}$$

where

$$n_0 = 2e^{\beta\mu}/(1+2e^{\beta\mu}). \tag{4.18}$$

The factor n (electron concentration) involved in the expressions for $\langle B^{+-}\rangle_0$ and $\langle F^{\sigma 0}\rangle_0$ and in formula (4.17) appears because of averaging over the distribution of nN localised electrons in N lattice sites. Such averaging is necessary because the zero-approximation Hamiltonian corresponds to a system with non-interacting states on different sites and the ground state of such a system is degenerate with respect to the electron configurations on the lattice.

Expression (4.16) can be transcribed into

$$\chi(k) \equiv -\mathcal{D}_\perp(k) = \chi_0(k)/\{[1-\Lambda(k)][1-Q(k)] + \chi_0(k)[\Phi(k)+J(\boldsymbol{k})]\} \tag{4.19}$$

where

$$\chi_0(k) = \tfrac{1}{2}(nn_0/T)\delta_{\omega_n,0} - \Pi(k). \tag{4.20}$$

On performing the analytical continuation $i\omega_n \to \omega + i\delta$, $\chi(\boldsymbol{k};\omega)$ is the dynamic susceptibility of the paramagnetic phase. The quantity $\chi_0(\boldsymbol{k};\omega)$ is a sum of independent contributions to the susceptibility by localised and itinerant states. The localised contribution is the usual Curie susceptibility (the first term in equation (4.20)). The quantity $-\Pi(k)$ represents the Pauli susceptibility of a free-electron gas. The denominator in the expression for $\chi(\boldsymbol{k};\omega)$ allows for the effect of the interaction of elementary magnetism carriers in the system. An effective parameter of this interaction is the quantity $(\Phi(k)+J(\boldsymbol{k}))$.

The quantities Π, Q, Λ and Φ involved in equation (4.19) have a formal smallness parameter $1/z$, where z is the number of nearest neighbours. To the quantity $\Phi(k)$ we add $J(\boldsymbol{k})$, which has no smallness $1/z$ but contains another smallness parameter, κ. If, in the calculation of the four-leg diagram, we had included the fourth bare vertex from expressions (4.1), this would have led to 'dressing' of the loops and to the occurrence of correction terms of order $\kappa(1/z)$. Therefore, the rejected part of the ladder diagrams with antiparallel lines in the four-leg diagram corresponds to the conditions

$$\kappa(1/z) \ll 1/z, \kappa \ll 1. \tag{4.21}$$

Formula (4.19) resembles the well known result due to Izuyama, Kim and Kubo [16], obtained for $\chi(\boldsymbol{k};\omega)$ in the opposite limit, $U \ll t$. However, this similarity is rather formal and comes from the random-phase approximation being used in both cases. A substantial distinction is that in [16] the denominator for $\chi(k)$ involves the expression $1 - U\chi_0(k)$, whereas in our case it contains, instead of U, another parameter, namely $\Phi(k) + J(\boldsymbol{k})$.

Finally, a crucial distinctive feature is that in our case ($U \gg t$) the expression for $\chi_0(k)$ involves a contribution by localised magnetic states, while in [16] $\chi_0(k) = -\Pi(k)$.

The Green function of the longitudinal components can be calculated in a similar fashion. It is determined by a four-leg diagram which should be found from the equations

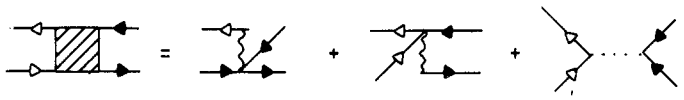

(4.22)

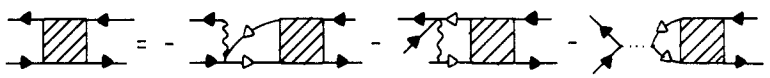

(4.23)

We label these four-leg diagrams Γ^{-+} and Γ^{++}, respectively. Solving equations written in the standard notation, we arrive at the following result for the paramagnetic phase:

$$\Gamma^{-+}(k_1 - k, k_1; k_2 + k, k_2) = [1/d_{\parallel}(k)][\varepsilon(\boldsymbol{k}_1 - \boldsymbol{k})\varepsilon(\boldsymbol{k}_2 + \boldsymbol{k}) \times \Pi(\Lambda + Q + J\Pi) + \varepsilon(\boldsymbol{k}_1 - \boldsymbol{k})(1 - Q^2 - \Pi\Phi - JQ\Pi) + \varepsilon(\boldsymbol{k}_2 + \boldsymbol{k}) \times (1 - \Lambda^2 - \Pi\Phi - J\Lambda\Pi) + \Phi(\Lambda + Q) + J(1 + Q\Lambda)] \tag{4.24}$$

$$\Gamma^{++}(k_1 - k, k_1; k_2 + k, k_2) = -[1/d_{\parallel}(k)][\varepsilon(\boldsymbol{k}_1 - \boldsymbol{k})\varepsilon(\boldsymbol{k}_2 + \boldsymbol{k})\Pi(1 + Q\Lambda - \Pi\Phi) + \varepsilon(\boldsymbol{k}_1 - \boldsymbol{k})(\Lambda - \Lambda Q^2 + Q\Pi\Phi + J\Pi) + \varepsilon(\boldsymbol{k}_2 + \boldsymbol{k})(Q - Q\Lambda^2 + \Lambda\Pi\Phi + J\Pi) + \Phi(1 - \Pi\Phi + Q\Lambda) + J(Q + \Lambda + J\Pi)] \tag{4.25}$$

where

$$d_{\parallel}(k) = [(1 - \Lambda)(1 - Q) - \Pi(\Phi + J)][(1 + \Lambda)(1 + Q) - \Pi(\Phi - J)]. \tag{4.26}$$

In these expressions the quantities Π, Q, Λ, Φ and J are functions of k; they are defined by formulae (4.6), in which the spin index of the electron Green functions should be omitted. The calculation here is more cumbersome than that for the transverse Green function. The final result is

$$\tfrac{1}{2}\mathcal{D}_{\parallel}(k) = \frac{(1/T)(\partial\langle B^{+-}\rangle_0/\partial\lambda_{\uparrow})\delta_{\omega_n,0} - \Pi(k)}{[1 - \Lambda(k)][1 - Q(k)] + [(1/T)(\partial\langle B^{+-}\rangle_0/\partial\lambda_{\uparrow})\delta_{\omega_n,0} - \Pi(k)][\Phi(k) + J(k)]}. \tag{4.27}$$

Taking account of the expression for the cumulant involved here,

$$(\partial\langle B^{+-}\rangle_0/\partial\lambda_{\uparrow})|_{\lambda_{\uparrow}=0} = \tfrac{1}{2}nn_0 \tag{4.28}$$

we come to the conclusion that formulae (4.27) and (4.16) for the transverse and longitudinal Green functions in the paramagnetic phase coincide (to within a sign and a numerical coefficient $\frac{1}{2}$), as should be the case.

5. Instability of the paramagnetic phase: phase diagram

In expressions (4.6), defining the major quantities upon which the final result (4.19) depends, we can carry out a summation over frequencies to obtain

$$T\sum_n G^0_\uparrow(k_1-k)G^0_\downarrow(k_1) \Rightarrow \{f[\xi(\boldsymbol{k}_1-\boldsymbol{k})]-f[\xi(\boldsymbol{k}_1)]\}/\{\xi(\boldsymbol{k}_1-\boldsymbol{k})-\xi(\boldsymbol{k}_1)-\mathrm{i}\omega_n\} \tag{5.1}$$

where $\xi(\boldsymbol{k}) = (1-\frac{1}{2}n)\varepsilon(\boldsymbol{k}) - \mu$. The expression thus obtained enables us to investigate the behaviour of the quantities $\Pi(k)$, $Q(k)$, $\Lambda(k)$ and $\Phi(k)$ with different $\boldsymbol{k}$, $\mathrm{i}\omega_n = 0$.

To investigate the instability of the paramagnetic phase with respect to antiferromagnetism, we consider $\chi(k)$ at $\boldsymbol{k} = \boldsymbol{k}_0 = (\pi,\pi,\pi)/a$ and zero frequency. In this case

$$\varepsilon(\boldsymbol{k}-\boldsymbol{k}_0) = -\varepsilon(\boldsymbol{k}). \tag{5.2}$$

The sums over $\boldsymbol{k}$ in expressions (4.6) may be expressed in terms of integrals over the energy ε with the density of states $\rho_0(\varepsilon)$. On the assumption that $\rho_0(\varepsilon)$ is symmetric, i.e. $\rho_0(\varepsilon) = \rho_0(-\varepsilon)$, it can be shown that at $T = 0$

$$\Pi(\boldsymbol{k}_0,0) = \frac{1}{1-\frac{1}{2}n}\int_{-\infty}^{\tilde{\varepsilon}_F} \mathrm{d}\varepsilon\,\frac{\rho_0(\varepsilon)}{\varepsilon} \qquad \Phi(\boldsymbol{k}_0,0) = -\frac{1}{1-\frac{1}{2}n}\int_{-\infty}^{\tilde{\varepsilon}_F}\mathrm{d}\varepsilon\,\varepsilon\rho_0(\varepsilon)$$
$$\Lambda(\boldsymbol{k}_0,0) = -Q(\boldsymbol{k}_0,0) = 0 \tag{5.3}$$

where $\tilde{\varepsilon}_F = \varepsilon_F(1-\frac{1}{2}n)^{-1}$ and ε_F is the Fermi energy. The latter should be found from the equation for the chemical potential

$$\tfrac{1}{2}n = (1-\tfrac{1}{2}n)\int_{-\infty}^{\infty}\mathrm{d}\varepsilon\,\rho_0(\varepsilon)f(\xi) \tag{5.4}$$

taken at $T = 0$.

We adopt a rectangular band model for which

$$\rho_0(\varepsilon) = \frac{1}{W}\begin{cases}1 & -\frac{1}{2}W < \varepsilon < \frac{1}{2}W \\ 0 & -\frac{1}{2}W > \varepsilon > \frac{1}{2}W\end{cases} \qquad \varepsilon_F = \tfrac{1}{2}W(\tfrac{3}{2}n-1) \tag{5.5}$$

with $W = 2zt$ being the width of a band with an $\varepsilon(\boldsymbol{k})$ spectrum. From expressions (5.3), it follows that

$$\Pi(\boldsymbol{k}_0,0) = \frac{1}{1-\frac{1}{2}n}\frac{1}{W}\ln\left(\frac{1-\frac{3}{2}n}{1-\frac{1}{2}n}\right) \qquad n < n_c = \tfrac{2}{3} \tag{5.6}$$

$$\Phi(\boldsymbol{k}_0,0) = \tfrac{1}{4}[n(1-n)/(1-\tfrac{1}{2}n)^3]W. \tag{5.7}$$

To determine the stability boundary of the paramagnetic phase, we explore the expression

$$\chi(k_0,0) = \frac{\frac{1}{2}nn_0 - T\Pi(\boldsymbol{k}_0,0)}{T + [\frac{1}{2}nn_0 - T\Pi(\boldsymbol{k}_0,0)][\Phi(\boldsymbol{k}_0,0) - \kappa tz]}. \tag{5.8}$$

Since for $T = 0$, $n_0 = 0$ at $\varepsilon_F < 0$ and $n_0 = 1$ at $\varepsilon_F > 0$, we need to consider two cases:

(i) $\varepsilon_F < 0$. Because $\Pi(\boldsymbol{k}_0,0) < 0$, the condition for the paramagnetic phase

$\chi(\boldsymbol{k}_0, 0) < 0$ to be unstable at $T = 0$ has the form

$$1 - \Pi(\boldsymbol{k}_0, 0)[\Phi(\boldsymbol{k}_0, 0) - \kappa tz] < 0. \tag{5.9}$$

This condition can be fulfilled if

$$\Phi(\boldsymbol{k}_0, 0) - \kappa tz < 0. \tag{5.10}$$

(ii) $\varepsilon_F > 0$. The paramagnetic phase is unstable if condition (5.10) is satisfied. For the rectangular band, conditions (5.9) and (5.10) read

$$\kappa > \tfrac{1}{2}n(1-n)/(1-\tfrac{1}{2}n)^3 \qquad \tfrac{2}{3} < n < 1 \tag{5.11}$$

$$-\frac{1}{2-n}\left(\kappa - \frac{1}{2}\frac{n(1-n)}{(1-\frac{1}{2}n)^3}\right)\ln\left(\frac{1-\frac{3}{2}n}{1-\frac{1}{2}n}\right) > 1 \qquad n < \tfrac{2}{3}. \tag{5.12}$$

The instability of the paramagnetic state relative to ferromagnetism is determined from the quantity $\chi(k, 0)$ at $\boldsymbol{k} = 0$:

$$\chi(0,0) = \frac{\frac{1}{2}nn_0 - T\Pi(0,0)}{T[1 - Q(0,0)]^2 + [\frac{1}{2}nn_0 - T\Pi(0,0)][\Phi(0,0) + \kappa tz]} \tag{5.13}$$

where

$$\Pi(0,0) = -\frac{1}{(1-\frac{1}{2}n)}\rho_0(\tilde{\varepsilon}_F) \qquad \Phi(0,0) = -\frac{1}{(1-\frac{1}{2}n)}\tilde{\varepsilon}_F^2\rho_0(\tilde{\varepsilon}_F)$$
$$\Lambda(0,0) = Q(0,0) = -[1/(1-\tfrac{1}{2}n)]\tilde{\varepsilon}_F\rho_0(\tilde{\varepsilon}_F). \tag{5.14}$$

It can be readily noticed that the paramagnetic phase is stable at $\varepsilon_F < 0$. With $\varepsilon_F > 0$ this phase is unstable if

$$\Phi(0,0) + \kappa tz < 0 \tag{5.15}$$

a condition which for the rectangular band implies that

$$\kappa < \tfrac{1}{2}(\tfrac{3}{2}n - 1)^2/(1 - \tfrac{1}{2}n) \qquad n > n_c = \tfrac{2}{3}. \tag{5.16}$$

On the basis of the analysis performed, we construct the phase diagram of the magnetic states on the (κ, n) plane (figure 3). Here the line f corresponds to condition (5.16), the line a to condition (5.11), and the line a′ to condition (5.12), when the inequality sign is replaced by an equality sign. As we see, magnetic states arise when the

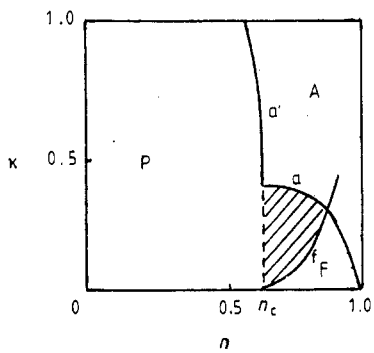

Figure 3. Magnetic phase diagram for (t–J) model.

Hubbard band is filled near the upper edge: at $n_c < n < 1$ for the ferromagnetic phase and virtually in the same interval of n for the antiferromagnetic phase. Antiferromagnetism arises at large values of κ. As κ is increased the antiferromagnetic region expands considerably. It should, however, be kept in mind that *per se* the (t–J) model holds good only for $\kappa \ll 1$.

Inspection of figure 3 shows also that with $n \simeq 0.97$ the phase boundaries f and a intersect, thereby indicating that a phase region exists in which the F and A phases coexist. However, it should be borne in mind that in this concentration range (almost half-filled band) allowance for the interaction of holes with spin deviations is of crucial importance. This follows from a paper by Nagaoka [6], who has given an exact stability criterion for the ferromagnetic state at $\kappa \ll 1$ and $(1 - n) \ll 1$ (for this problem, see also [4]). For the first time, the importance of taking into account the electron–magnon interaction in the Hubbard model has been explicitly indicated in [18]. For this reason, the analogue of the random-phase approximation that we exploit needs to be refined both in the vicinity of $n = 1$ and in the evaluation of the critical concentration n_c.

The shaded region between the lines restricting the A and F phases corresponds apparently to a more complicated ordering. The authors of [19] argue that this region may contain heterogeneous phases which represent an antiferromagnetic structure with inclusions of ferromagnetic regions that are due to holes.

6. Conclusions

The major physical result of the present paper resides in the derivation of the dynamic susceptibility of the (t–J) model, expressed by formula (4.19) with formula (4.20). These formulae reflect the dual nature of the magnetic states in the Hubbard model, the duality manifesting itself in the presence of a localised and an itinerant contribution. The relative magnitude of the localised contribution, which has the character of the Curie susceptibility, is determined by the parameter n_0, which varies between 0 and 1 as the electron concentration n is varied. At low temperatures this variation comes about sharply at $n = n_c = \frac{2}{3}$. Formula (4.20) shows that when $n < n_c$ the localised contribution is suppressed and the system behaves mainly as an itinerant magnet. With $n > n_c$, a Curie-type contribution appears in the zero susceptibility. Owing to this contribution the system acquires features of a Heisenberg magnet in which a particular magnetic ordering type arises if the magnetic correlation parameter $\Phi(k) + J(\boldsymbol{k}) < 0$.

The dual nature of the magnetic states in the Hubbard model is a reflection of the mathematical fact that the commutator or anticommutator of two Hubbard operators is not a c-number. In this situation both Fermi-type and Bose-type one-particle Green functions have a complicated structure, which contains terminal diagrams. Relations (3.13) and (3.19) for Green functions of transverse and longitudinal components are general fundamental graphic equations for Green functions composed of Hubbard operators. The terminal diagrams are highly essential, and only consistent allowance for these diagrams along with the usual Dyson part of the Green function leads to the correct result. Without the diagram technique developed in this paper (by invoking, for example, the decoupling procedure), the general mathematical structure of the Green functions, expressed by relations (3.13) and (3.19), would have been extremely difficult to reveal.

Concrete calculations have been provided within the framework of an approximation that consists of summing for the electron four-leg diagram ladder-type diagrams with antiparallel electron lines. In the given situation this reduces to summing diagrams with

different simple loops that have the same momentum, in the spirit of the non-interacting modes approximation. This approximation leads to a sufficiently simple expression for the magnetic susceptibility and thus makes it possible to obtain the magnetic phase diagram of the model. The diagram technique formulated here permits the study of the various properties of the (t–J) model. The superconducting state that arises within the framework of this model will be investigated in a subsequent paper.

Acknowledgment

The authors are indebted to Dr V Yu Irkhin for helpful discussions.

References

[1] Hubbard J 1963 *Proc. R. Soc.* A **276** 238
[2] Roth L 1969 *Phys. Rev.* **184** 451
[3] Sokoloff J 1970 *Phys. Rev.* B **2** 3707
[4] Nikolaev M Yu, Ryzhanova N V, Vedyaev A V and Zubritskii S M 1985 *Phys. Status Solidi* b **128** 513
[5] Nolting W and Borgiel W 1989 *Phys. Rev.* B **39** 6962
[6] Nagaoka Y 1966 *Phys. Rev.* **147** 392
[7] Zaitsev R O 1976 *Sov. Phys.–JETP* **43** 574
[8] Zaitsev R O 1977 *Sov. Phys.–Solid State* **19** 1874
[9] Slobodyan P M and Stasyuk I V 1974 *Theor. Math. Phys.* **19** 616
[10] Vedyaev A V and Nikolaev M Yu 1984 *Theor. Math. Phys.* **59** 293
[11] Westwanskii B 1973 *Phys. Lett.* A **44** 27
[12] Izyumov Yu A and Skryabin Yu N 1988 *Statistical Mechanics of Magnetically Ordered Systems* (New York: Consultants Bureau)
[13] Anderson P W 1987 *Science* **235** 1196
[14] Vaks V G, Larkin A I and Pikin S A 1968 *Sov. Phys.–JETP* **26** 188
[15] Abrikosov A A, Gorkov L P and Dzyaloshinskii I E 1975 *Methods of Quantum Field Theory in Statistical Physics* (New York: Dover)
[16] Izuyama T, Kim D and Kubo R 1963 *J. Phys. Soc. Japan* **18** 1025
[17] Bar'yakhtar V G, Krivoruchko V N and Yablonskii D A 1984 *Sov. Phys.–JETP* **58** 351
[18] Hertz J A and Edwards D M 1973 *J. Phys. F: Met. Phys.* **3** 2174
[19] Visscher P B 1987 *Phys. Rev.* B **35** 6694
Auslender M I and Katsnelson M I 1982 *Theor. Math. Phys.* **51** 436